Resonant Converters for Electric Equipment Power Supply

Maria Teresa Outeiro, *Member, IEEE*
IPC/ISEC, Coimbra, Portugal
ISR, Porto, Portugal
teresa.outeiro@fe.up.pt

Giuseppe Buja, *Life Fellow, IEEE*
DII, University of Padova
Padova, Italy
giuseppe.buja@unipd.it

Adriano Carvalho, *Member, IEEE*
FEUP, University of Porto
Porto, Portugal
asc@fe.up.pt

***Abstract* — The paper deals with the use of resonant converters for the power supply of electric equipment. After exploring the advantages of using the resonant conversion, an analysis of the three main resonant topologies, namely i) series-resonant, ii) parallel-resonant, and iii) a combination of them, is carried out and a series resonant converter is implemented. Considerations on the design of the resonant converter as well as on the selection of their components, including the HF transformer, are presented. Performance of the implemented series resonant converter is investigated in terms of dynamic behavior through experimental results.**

***Keywords* — Power supply, resonant topologies, switching mode, soft switching, component selection/design, dynamic and stability analysis.**

I. INTRODUCTION

The main requirements for the power supplies (PSs) are high reliability, high efficiency, small size, long life, low EMC and low cost. Order of importance and quantitative specifications for the various requirements are application-dependent. In any case, certain compromises in meeting the requirements must be accepted when designing a PS [1]. Recently, attention has been paid to techniques and methods of improving the efficiency; this has been achieved through the arrangement of suitable topologies, use of technology-advanced power switches and introduction of sophisticated control systems [2], [3]. The choice of the topology is typically related to the output power level required by the application. However this criterion by itself is generally insufficient and can lead to inadequate efficiency performance and unreliable design. As a matter of fact, besides the output power level, other important and even critical parameters and/or requests can be taken into account, including input voltage and range, output voltage and current levels, load type, isolation criteria, magnetics components utilization and packaging.

As mentioned above, efficiency is today the most important challenge in designing a PS. The technical solution devised to set up an high-efficiency PS is soft switching that is implemented through on-purpose developed power circuitry, i.e. the resonant converters. After an overview of the different switching topologies, the paper specifically deals with the resonant converters when used for the power supply of electric equipment.

II. POWER SUPPLY TOPOLOGIES

Any topology can be used to implement a PS; however, each topology has its own unique features, which make it suited for certain applications. To select the most suitable topology for a given specification, it is essential to know the operation of the topologies together with their advantages, drawbacks, complexity and area of usage. The following factors can help in selecting the appropriate topology:

- Number of outputs required;
- Output voltage level with respect to the input one;
- Need of an input/output galvanic isolation;
- Input/output voltage magnitude;
- Input/output current magnitude;
- Maximum voltage applied across the HF-transformer and maximum duty-cycle.

A PS contains networks made of energy storage elements, such as inductors and capacitors, and of power transistors and diodes. Their particular connection defines the topology. The development of new topologies for the PSs has been evolved in parallel to the advancements in the technology of materials and devices [4] as well as in the theory of the control systems [5], [6]. According to the operating mode, there are three basic PS types: 1) linear, 2) switching-mode, and 3) soft-switching or resonant.

While having advantages of simplicity, low noise, fast response time and excellent regulation, the linear PSs exhibit low efficiencies. In turn, the hard-switching PSs offer the advantage of reducing the conduction losses of the devices and, hence, of improving the PS efficiency even if the improvement is partly impaired by the high switching losses. Furthermore, they require additional circuitry to attenuate the harmonics produced by the switching but this is conveniently achieved by using small-size filters since the harmonics are in the range of tens of kHz. On the other side, the hard-switching PSs have the merit that the HF-transformer that isolates the power supply from the load is built up with light ferrite core.

Any PS operating in switching-mode (SMPS) solicits the switches with electrical stresses and energy losses that increase linearly with the switching frequency; moreover, it produces significant electromagnetic interferences due to the large values

of *di/dt* and *dv/dt* occurring across the circuital components. Snubber circuits in series and/or in parallel with the switches are usually needed to limit these inconveniences.

In order to increase the switching frequency and, at the same time, to reduce the shortcomings of the SMPS, resonance conversion techniques are used [7], [8], [9]. A schematic of the resonant converters showing different resonant tank networks (RTNs) is illustrated in Fig. 1. Although any topology can be used in the controlled switch network (CSN), the half- or full-bridge configurations are commonly adopted. By connecting the inductive and capacitive elements of the RTN in series, parallel or combination of them, a resonance condition is produced allowing the increase of the switching frequency while reducing the losses through soft-switching operation. The HF-transformer is commonly used in applications requiring a high output voltage or an input/output galvanic isolation; for simplicity, it is not considered in the analysis of the resonant converter schemes.

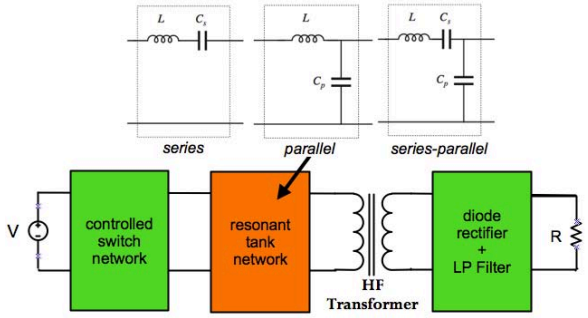

Fig. 1. Schematic of a resonant converter topology with HF-transformer.

III. RESONANT CONVERTER ANALYSIS

In this Section the properties of the series, parallel and series-parallel load resonant converters are analyzed and compared. The term load is often added to the name resonant converters since the load is part of the resonant circuit. Due to the RTN, harmonics of the switching frequency are negligible and the RTN quantities are nearly sinusoidal. This leads to the approximation of taking them as pure sine-waves.

The sinusoidal approximation allows the use of simple equivalent circuits for the analysis of the various stages of the resonant converter, namely the CSN, the RTN, and the diode rectifier (DR) with an in-cascade low-pass (LP) filter. The effective load resistance of the RTN is given by its output voltage divided by its output current. By using the principle of effective load resistance, it becomes relatively easy to analyze how the output voltage and efficiency of the resonant converter are influenced by the RTN elements or by the HF transformer.

A) Characteristics of the series-resonant converter

Fig. 2 shows the topology of a series resonant converter (SRC). The CSN produces a square-wave voltage output $v_S(t)$ whose frequency f_s is equal/close to the resonant frequency f_0. Due to the filtering action of the RTN and in accordance with the sinusoidal approximation, the current $i_R(t)$ at the output of the CSN is a sine wave of frequency f_s.

The current i_R is then rectified and conditioned by the in-cascade LP filter that here is constituted by the capacitor C_f. Thanks to the capacitor, the load is supplied by a DC current (I_o) that produces a DC voltage (V_o) across its terminals. By adjusting the frequency f_s, the amplitude of both the current through the RTN and the voltage at its output can be controlled.

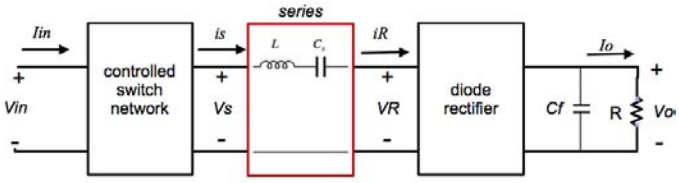

Fig. 2. SRC topology.

CSN equivalent circuit

The CSN is controlled to produce a square voltage $v_S(t)$ of frequency f_s (angular frequency $w_s=2\pi f_s$) that can be expressed by the Fourier series in (1). The current drawn by the RTN is primarily due to the fundamental frequency f_s of $v_S(t)$ while the current harmonics at the frequencies nf_s, with n= 3,5,7,… are greatly attenuated. Therefore only the power associated to the fundamental component of $v_S(t)$ is transferred from the CSN to the RTN and from it to DR and then to the load. Consequently, the output voltage of the CSN can be approximated with the fundamental harmonic $v_{S1}(t)$ in (2).

$$v_S(t) = \frac{4Vin}{\pi}\sum\frac{1}{n}\sin(nw_s t) \qquad with\ n = 1,3,5,7,\ldots \tag{1}$$

$$v_{S1}(t) = \frac{4Vin}{\pi}\sin(w_s t) \tag{2}$$

Note that $v_{S1}(t)$ has a peak amplitude of $(4/\pi)$ times the DC input voltage V_{in} and does not have any delay with respect to $v_s(t)$.

In the RTN the current is sinusoidal and can be represented by $i_S(t)$ with peak amplitude I_S and phase φ_S, that is by

$$i_S(t) = I_S\,sin\left(w_s t - \varphi_s\right) \tag{3}$$

The DC current I_{in} at the input of the CSN can be determined by averaging i_s over one half of the fundamental period, i.e. by

$$I_{in} = \frac{2}{T_s}\int_0^{\frac{Ts}{2}} i_s(t)dt = \frac{2}{\pi}I_S cos\left(\varphi_s\right) \tag{4}$$

Further to (2)-(4), the equivalent circuit reported in Fig. 3 is obtained for the CSN. The DC power supply with the input voltage V_{in} is converted into AC power with output voltage $v_S(t)$ having fundamental component $v_{S1}(t)$ and delivering an output current $i_{S1}(t)$.

DR equivalent circuit with capacitive output filter

The equivalent circuit of the DR with capacitive output

filter and in-parallel load resistor can be assessed by examining the behavior of the DR when entered by the current $i_R(t)$ that, due to the series connection, is equal to (3), i.e. it is

$$i_R(t) = i_s(t) \tag{5}$$

The current $i_R(t)$ is rectified by DR as shown in Fig.4, where $|i_R(t)|$ is the current flowing in the DC side of the DR. Due to the filtering action of the capacitor C_f, only the DC component of $|i_R(t)|$ flows into the load, producing the current I_o and the associated DC voltage V_o. At steady-state the DC component of $|i_R(t)|$ must be equal to the current I_o. Then

$$I_o = \frac{2}{T_s}\int_0^{\frac{T_s}{2}} i_R(t)dt = \frac{2}{\pi} I_R \tag{6}$$

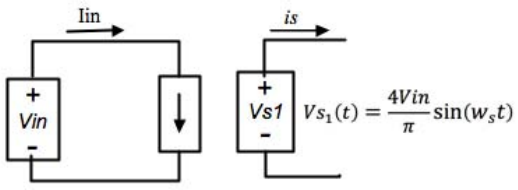

Fig. 3. CSN equivalent circuit.

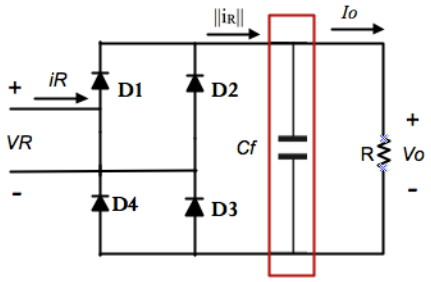

Fig. 4. DR with capacitive output filter.

The voltage $v_R(t)$ at the DR input can be simply obtained by observing that the conducting diodes of the DR change when the current $i_R(t)$ crosses zero. Then $v_R(t)$ has a square waveform whose value is V_o when $i_R(t)$ is positive and $-V_o$ when $i_R(t)$ is negative. Its Fourier series expressions is

$$v_R(t) = \frac{4Vo}{\pi}\sum\frac{1}{n}\sin(nw_s t - \varphi_s) \qquad with\ n = 1,3,5,7,\ldots \tag{7}$$

The voltage $v_R(t)$ can be also approximated by its fundamental component $v_{R1}(t)$ in (8) because of the RTN operation

$$v_{R1}(t) = \frac{4V_0}{\pi}\sin\left(w_s t - \varphi_s\right) \tag{8}$$

Note that $v_{R1}(t)$ has a peak amplitude of $(4/\pi)$ times the DC output voltage V_0 and is in phase with the current $i_R(t)$.

Since the voltage $v_{R1}(t)$ is in phase with $i_R(t)$, the input impedance to the DR is a pure resistance R_e, given by the ratio of $V_{R1}(t)$ to $I_R(t)$. By (6) and (8), it is

$$R_e = \frac{V_{R1}}{I_R} = \frac{\frac{4V_0}{\pi}}{\frac{\pi I_0}{2}} = \frac{8}{\pi^2}\frac{V_0}{I_0} = \frac{8}{\pi^2}R \tag{9}$$

Eq. (9) represents the effective load resistance of the RTN. By (5), (6), (8) and (9), the equivalent circuit of the DR with the capacitive output filter becomes as in Fig. 5 and the equivalent circuit of the whole SRC as in Fig. 6.

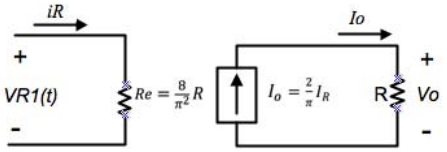

Fig. 5. DR equivalent circuit.

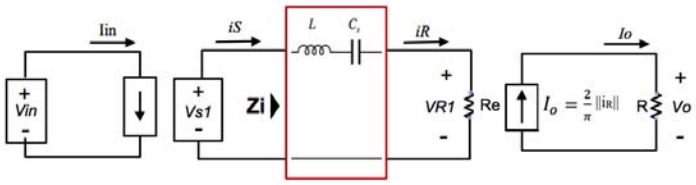

Fig. 6. SRC equivalent circuit with capacitive output filter.

Voltage tranfer function

The voltage transfer function can be divided into two contributions: one of the CSN and the other one of the RTN. As mentioned above, the CSN produces a square voltage at the frequency f_s but only its fundamental component $v_{S1}(t)$ determines the SRC behavior. Consequently the characteristics of the SRC can be evaluated by the equivalent circuit of Fig. 6. As it can be observed from the circuit, the effective load resistance R_e is in series with the LC components of the RTN so that, if the load increases, the current through the RTN decreases and viceversa. The impedance Z_i seen from the input terminals of the RTN and the voltage transfer function are respectively

$$Z_i = j\left(w_s L - \frac{1}{w_s C_s}\right) + R_e \tag{10}$$

$$\frac{\overline{V}_{R1}}{\overline{V}_{S1}} = \frac{R_e}{Z_i} = \frac{R_e}{R_e + j\left(w_s L - \frac{1}{w_s C_s}\right)} \tag{11}$$

As a function of the circuit elements, the following expressions can be found for the parameters of the SRC:

$$w_o = \frac{1}{\sqrt{LC_s}} = 2\pi f_0 \tag{12}$$

$$Z_0 = \sqrt{\frac{L}{C_s}} = w_0 L = \frac{1}{w_0 C_s} \tag{13}$$

$$Q_L = \frac{Z_0}{R_e} = \frac{w_0 L}{R_e} = \frac{1}{w_0 C_s R_e} = Q_s^{-1} \tag{14}$$

where w_0 is the resonant frequency, Z_0 is the characteristic impedance of the resonant circuit, Q_L is the load quality factor and Q_S is the normalized quality factor. By rearranging (11), the voltage gain for the SRC can be written as

$$\frac{V_{R1}}{V_{S1}} = \frac{1}{\sqrt{1+Q_L^2\left[\frac{f_s}{f_o}-\frac{f_o}{f_s}\right]^2}} \cong \frac{V_0}{V_{in}} \qquad (15)$$

Eq. (15) states that the DC voltage gain of the SRC is approximately equal to the AC voltage gain of the RTN evaluated at the switching frequency f_s. Fig. 7 plots (15) as a function of f_s/f_0 for various values of Q_L. The figure points out that

- The maximum voltage gain is unity.
- The voltage gain vs. f_s/f_0 increases for $f_s<f_0$ and decreases for $f_s>f_0$.
- To maintain a constant value of the voltage gain when Q_L decreases, f_s/f_0 has to be increased.
- For a given value of f_s/f_0, the voltage gain increases if Q_L decreases
- The switching frequency range required to maintain a constant voltage gain is very narrow at higher values of Q_L for both $f_s < f_o$ and $f_s > f_o$.

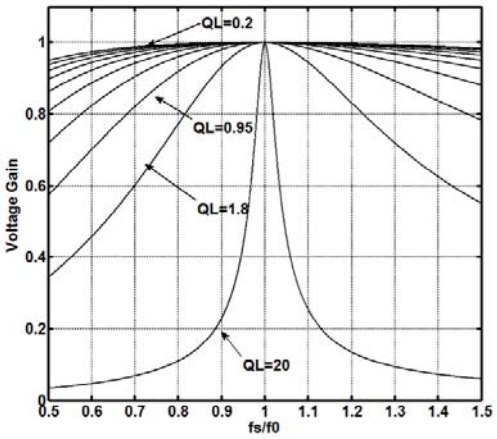

Fig. 7. Voltage gain vs. f_s/f_0 for the SRC.

B. Characteristics of the parallel-resonant converter

Fig. 8 shows the schematic of a parallel resonant converter (PRC). The topology differs from the SRC in two points: i) the resonant capacitor is in parallel with the DR, and ii) the DR drives an in-cascade LP filter of inductive type. Consequently the value of the effective load resistance R_e differs from that of the SRC. Like to the SRC, the sinusoidal approximation is made to analyze the characteristics of the PRC.

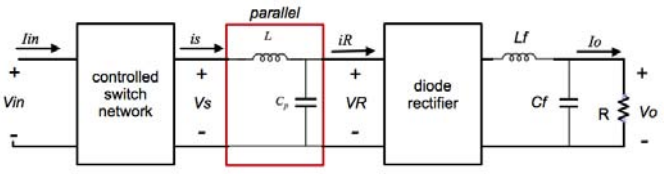

Fig. 8. PRC topology.

CSN equivalent circuit

The analysis of the CSN proceeds in a similar way as for the SRC. The CSN is controlled to generate a square-wave voltage $v_S(t)$ of frequency f_s. Therefore the same equations as (1) and (2) apply to $v_S(t)$, to its fundamental component and to the input DC current I_{in}, yielding again to the equivalent circuit of Fig. 3.

DR equivalent circuit with inductive output filter

The equivalent circuit of the DR with inductive output filter is analyzed by a dual approach of that used for the SRC. Here the rectifier input voltage is sinusoidal with amplitude V_R and phase shift φ_R as shown by

$$v_R(t) = V_R \sin\left(w_s t - \varphi_R\right) \qquad (16)$$

Then the DR is entered by a sinusoidal voltage and the input current $i_R(t)$ has a square waveform that is equal to $+I_0$ when $v_R(t)$ is positive and equal to $-I_0$ when $v_R(t)$ is negative. Since the conducting diodes of the DR change when the voltage $v_R(t)$ cross zero, the fundamental component $i_{R1}(t)$ of the current $i_R(t)$ is in phase with $v_R(t)$. The rectifier input current can be expressed in Fourier series by (17) and its fundamental component is given by (18).

$$i_R(t) = \frac{4I_o}{\pi}\sum\frac{1}{n}\sin(nw_s t - \varphi_R) \qquad with\ n = 1,3,5,7,\ldots \qquad (17)$$

$$i_{R1}(t) = \frac{4I_0}{\pi}\sin\left(w_s t - \varphi_R\right) \qquad (18)$$

Note that $i_{R1}(t)$ has a peak amplitude of $(4/\pi)$ times the DC output current I_0 and, as anticipated, has the same phase of $v_R(t)$.

The rectifier output voltage $|v_R(t)|$ is filtered by the inductor L_f. In steady-state the DC component of $|v_R(t)|$ has the value of

$$V_o = \frac{2}{T_s}\int_0^{\frac{T_s}{2}} v_R(t)dt = \frac{2}{\pi}V_R \qquad (19)$$

and is equal to the load voltage V_0. In this case, the DR offers to the RTN an effective load resistance R_e given by the ratio of $v_R(t)$ to $i_{R1}(t)$, i.e. by

$$R_e = \frac{V_R}{i_{R1}} = \frac{\frac{\pi V_o}{2}}{\frac{4I_o}{\pi}} = \frac{\pi^2}{8}\frac{V_o}{I_o} = \frac{\pi^2}{8}R \qquad (20)$$

Accordingly, the equivalent circuit of the DR with inductive output filter becomes as in Fig. 9 and the equivalent circuit of the whole PRC as in Fig. 10.

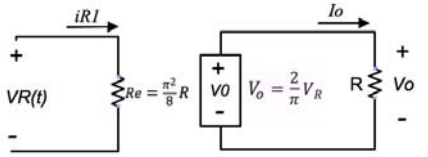

Fig. 9. DR equivalent circuit with inductive output filter.

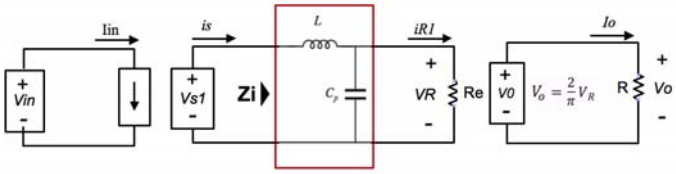

Fig. 10. PRC equivalent circuit.

Voltage transfer function

The voltage transfer function of the PRC can be evaluated from the equivalent circuit of Fig. 10. The effective load resistance R_e is in parallel to the resonant capacitor C_p so that, if R_e is much higher than the reactance of C_p, the current through the resonant inductor and the CSN is almost independent from the load. Moreover, the voltage across C_p as well as across the load rises as R_e increases. The impedance Z_i as seen from the input terminals of the RTN and the voltage transfer function are respectively

$$Z_i = X_L + Z_{eq}; \qquad Z_{eq} = \left(X_{Cp} // R_e\right) = \frac{\frac{R_e}{jw_S C_p}}{R_e + \frac{1}{jw_S C_p}} \tag{21}$$

$$\frac{\overline{V}_R}{\overline{V}_{S1}} = \frac{X_{Cp} // R_e}{X_L + \left(X_{Cp} // R_e\right)} = \frac{\frac{R_e}{1 + jw_S C_p R_e}}{jwL + \frac{R_e}{1 + jw_S C_p R_e}} \tag{22}$$

As a function of the circuit elements, the following expression can be found for the parameters of the PRC:

$$w_o = \frac{1}{\sqrt{LC_p}} = 2\pi f_0 \tag{23}$$

$$Z_o = \sqrt{\frac{L}{C_p}} = w_0 L = \frac{1}{w_0 C_p} \tag{24}$$

$$Q_L = \frac{R_e}{Z_0} = w_0 C_p R_e = \frac{R_e}{w_0 L} = Q_p \tag{25}$$

By rearranging (22), the voltage gain for the PRC can be written as

$$\frac{V_R}{V_{S1}} = \frac{1}{\sqrt{\left[1 - \left(\frac{f_S}{f_O}\right)^2\right]^2 + \left[\frac{f_S}{f_O}\left(\frac{1}{Q_L}\right)\right]^2}} \cong \frac{V_o}{V_{in}} \tag{26}$$

Fig. 11 plots (26) as a function of f_s/f_0 for various values of Q_L. The figure points out that

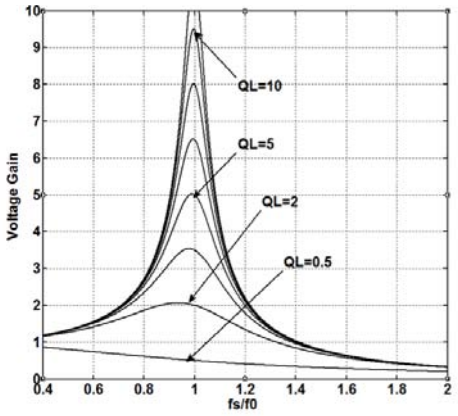

Fig. 11. Voltage gain vs. f_s/f_0 for the PRC.

- At switching frequencies near the resonant frequency (i.e. for $f_s \cong f_0$) and for values of Q_L of a few units, the gain increases sharply. Then the output voltage rises to very high values at no-load (or for light loads) if the switching frequency is not properly controlled.

C. Characteristics of the series-parallel resonant converter

Fig. 12 shows the topology of a series-parallel resonant converter (SPRC). The topology combines the advantages of those of the SRC and the PRC while eliminating their weak points such as i) poor load voltage control at high loads in the SRC and ii) RTN-circulating current independent from the load in the PRC. The objectives are achieved by the appropriate selection of both the resonant elements and the switching frequency.

In the SPRC, the RTN is made of two branches: one in series made of the capacitor C_s and the inductor L and one in parallel made of the capacitor C_p. The DR has an in-cascade LP filter of inductive type like in the PRC.

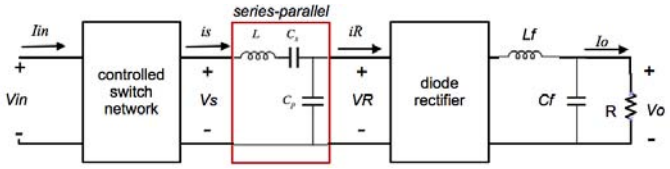

Fig. 12. SPRC topology.

Proceeding in a similar way as for the PRC, it turns out that the voltage $v_R(t)$ is approximately sinusoidal whilst the current $i_R(t)$ has a square waveform with the fundamental component $i_{R1}(t)$ still given by (18). Therefore the equivalent circuit of the SPRC can be represented as in Fig. 13.

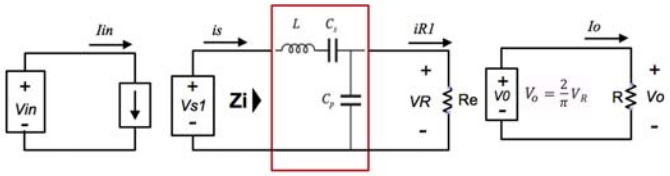

Fig. 13. SPRC equivalent circuit.

Voltage transfer function

The voltage transfer function of the SPRC can be evaluated from the equivalent circuit of Fig. 13. From the circuit, the impedance Z_i seen from the input terminals of the RTN and the voltage-transfer function can be calculated as

$$Z_i = X_L + X_{Cs} + \left(X_{Cp} // R_e\right) = j\left(w_s L - \frac{1}{w_s C_s}\right) + \frac{\frac{R_e}{jw_S C_p}}{Re + \frac{1}{jw_S C_p}} \tag{27}$$

$$\frac{\overline{V}_R}{\overline{V}_{S1}} = \frac{X_{Cp} // R_e}{X_L + X_{Cs} + \left(X_{Cp} // R_e\right)} = \frac{\frac{R_e}{1 + jw_S C_p R_e}}{j\left(w_s L - \frac{1}{w_S C_S}\right) + \frac{R_e}{1 + jw_S C_p R_e}} \tag{28}$$

As a function of the circuit elements, the following expressions can be found for the parameters of the SPRC:

$$w_0 = \sqrt{\frac{1}{LC_{eq}}} \tag{29}$$

$$Q_L = Q_{sp} = \frac{R_e}{w_0 L} = w_0 C_{eq} R_e; \;\; C_{eq} = \frac{C_S C_p}{C_S + C_p} \tag{30}$$

By rearranging (28), the voltage gain for the SPRC can be written as

$$\frac{V_R}{V_{S1}} = \frac{1}{\sqrt{(1+A)^2\left[1-\left(\frac{f_S}{f_O}\right)^2\right]^2+\left[\frac{1}{Q_L}\left(\frac{f_S}{f_O}-\frac{f_O}{f_S}\frac{A}{A+1}\right)\right]^2}} \cong \frac{V_o}{V_{in}} \quad (31)$$

where

$$A = \frac{C_p}{C_s} \quad (32)$$

Fig. 14 plots (31) as a function of f_s/f_0 for various values of Q_L. The figure points out that

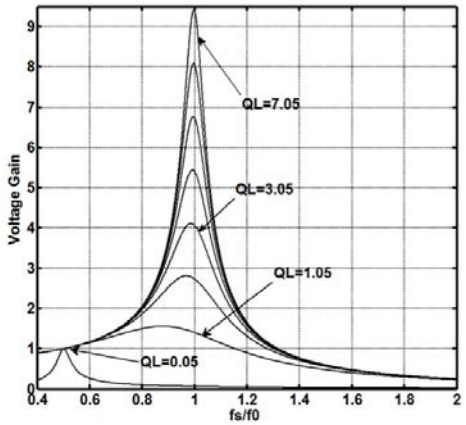

Fig. 14. Voltage gain vs. f_s/f_0 for the SPRC.

- The SPRC operates like the PRC for frequencies close to f_0.
- At the resonant frequency f_r of the brach made of the series of L and C_s, the SPRC operates as the SRC with maximum voltage gain equal to unity.
- For $f_s<f_0$ the RTN appears as a capacitive load to the CSN, i.e. the RTN input current leads the fundamental component of the voltage generated by the CSN. The opposite occurs for $f_s>f_0$.

D. Benefits of using resonant converters in PS

In the previous Section, resonant converters with different topologies have been analyzed. Each of them has its own features. For instance, the SRC can be easily used with a full-bridge CSN without any control of the unbalance in the switching times of and the forward voltage drops across the power devices since the DC current is kept out from the HF-transformer. Moreover, the currents in the power devices reduce as the load decreases. This means that the conduction losses of the power devices reduce as the load decreases, thus maintaining high efficiency. The main disadvantage of the SRC is concerning with its capability to regulate the output voltage in case of no-load or very light loads (Fig. 7). Consequently, the SRC is not a good choice for applications requiring a voltage regulation with light loads.

The PRC is inherently short-circuit proof (Fig. 11). This makes it particularly attractive under severe short-circuit requirements. The PRC is also a good option for applications with relatively low input voltage range and/or with nearly constant loads around its maximum power design point.

The SPRC puts together the advantages of the SRC and the PRC (Fig. 14) and then is a good selection for a large field of applications despite its complex arrangement.

IV. SERIES RESONANT CONVERTER APPLICATION

Due its simplicity and benefits, a 1 kW SRC prototype has been designed and implemented for a PEM fuel cell application. The constraints imposed by the PEM on the PS and the requirements for the SRC are summarized in Tables I and II respectively.

Table I - Constraints imposed by the PEM Mark1020 on the PS

I_{fc} (A)	V_{fc} (V)	Power (W)
2.8	23.71	66
24	19.11	492

Table II – SRC requirements

Description	Parameter	Mark1020
Power to transfer to load	P_{out} (W)	66.39 – 492
Output voltage required	V_{out} (V)	48
Output current	I_{out} (A)	0.26 – 2.2
Voltage output ripple	ΔV_{out} (V)	≤ 2%
Ripple current to the PEM	ΔI_{PEM} (A)	No Ripple

The circuitry of the SRC for the fuel cell application is shown in Fig. 15. Note that i) the circuitry has a filter located at the output of the fuel cell to smooth the current delivered by it, ii) the CSN has a full-bridge scheme, and iii) the equivalent load resistance R_e of the SRC is the sum of the HF-transformer resistance and the load referred to its primary side.

The SRC operates in discontinuous conduction mode at frequencies below the resonant frequency ($f_s<f_0$) with zero-current switching (ZCS). The RTN offers a capacitive load to the CSN and this enables natural commutation of the power switches with the consequential elimination of the switching losses.

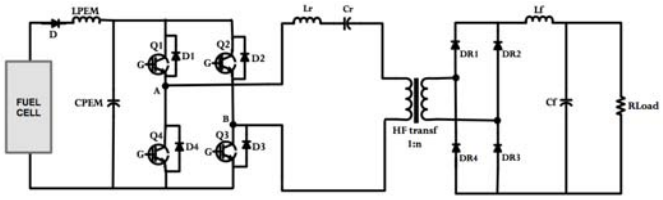

Fig. 15. SRC circuitry for the fuel cell application.

A. SRC design and implementation

Beside an accurate selection of the power devices, of the fuel cell filter and of the SRC output filter, a special attention has been set on the design of the resonant circuit and the HF-transformer.

The criteria posed for the resonant components were as follows: i) an inductor as small as possible to limit the

switching transient voltages, and ii) a capacitor able to transfer the required power at the switching frequency of the SRC. As a matter of fact, requirements for the capacitor were more stringent and included the need of supporting high peak voltages, of tolerating large current ripple, of working over a large temperature range and of being stable in the time. Accordingly a capacitor of HVDC technology has been used.

The value for the resonant inductor L_r was set at the total leakage inductance of the HF-transformer referred to the primary. Its inductance is resulted in 2.1µH. The value for the resonant capacitor C_r was of 4µF for a resonance frequency of 56 kHz.

The size of the HF-transformer depends on the power to be transferred as well as on the operating frequency. As the frequency increases, the size diminishes. If the CSN operates at a frequency close to the resonant frequency, the maximum power transfer takes place. An important point in the HF-transformer design is the choice of the magnetic material for the core that must be of ferrite type to keep low the parasitic losses. Here the N27 ferrite has been used. Table III summarizes the main characteristics of the components of the implemented SRC.

Table III – SRC components.

Converter part	**References and values**
IGBT module (EUPEC)	F4 -5012MS4
Ultra fast diodes (ST-Microelectronics)	BYV225V -200
HF-Transformer: 1:n, core type	1:10, Ferrite, type EE
PEM filter: L_{PEM} , C_{PEM} , frequency	933 µH, 940 µF, 170 Hz
Output filter: L_f, C_f, frequency	740 µH, 110 µF, 557 Hz

V. EXPERIMENTAL RESULTS

Experiments on the implemented SRC have been focused on its dynamic behavior. Some significant results are reported in Figs. 16 and 17. As Fig. 16 shows, the SRC reacts to a slow variation of the load by updating its switching frequency so as to transfer the required power from the fuel cell to the load. As Fig. 17 shows, the SCR reacts to a steeply reduction of the load by a very fast update of its switching frequency to keep the load voltage regulated at the required value. The experimental results demonstrate that the implemented SCR exhibits excellent dynamic performance.

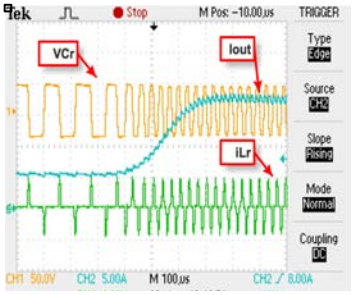

Fig. 16. SRC resonant frequency variation in response to slow load variation.

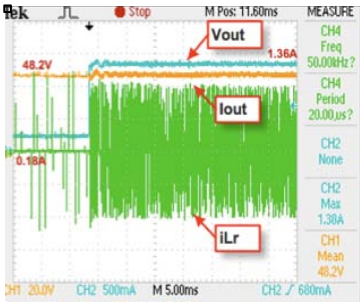

Fig. 17. SRC response to a load step-down.

VI. CONCLUSIONS

The paper has dealt with the resonant converters used in the PS of electric equipment. After describing the advantages of the resonant conversion, an analysis of the three basic resonant converter topologies has been carried out, namely i) the SRC, ii) the PRC, and iii) the SPRC. Considerations on the design of a 1 kW SRC prototype and on the relevant components, including the HF transformer, are presented. Performance of the implemented SRC is investigated in terms of dynamic behavior obtaining excellent results.

ACKNOWLEDGMENT

The authors would like to thank *Fundação Luso-Americana para o Desenvolvimento (FLAD)* that supports this work.

REFERENCES

[1] M.T.Outeiro, R.Visintini, and G.Buja, "Considerations in Designing Power Supplies for Particle Accelerators", in Proc. of IEEE Industrial Electronics International Conference (IECON), 2013, pp.7074-7079.

[2] M. Emmenegger, H. Jäckle, R. Künzi, and S. Richner, "A new generation of digital power supply controllers", Presented at the 1st International Particle Accelerator Conference (IPAC2010), Kyoto, Japan, 2010, pp. 3263–3265.

[3] P. Nguyen and A. Gerth, "Soft switching with SiC-devices for compact onboard railway power supplies," in Proc. of 15th International Conference on Power Electronics and Motion Control (EPE/PEMC), 2012, pp. LS3c.1–1–LS3c.1–6.

[4] O. Mostaghimi, N.Wright, and A. Horsfall, "Design and Performance Evaluation of SiC Based DC-DC Converters for PV Applications", in Proc. of 4th Annual IEEE Energy Conversion Conference and Exposition, 2012, pp. 3956 – 3963.

[5] T.W. Ching and K.U.Chan, "Review of Soft-Switching Techniques for High-Frequency Switched-Mode Power Converters", in Proc. of IEEE Vehicle Power and Propulsion Conference (VPPC), 2008, pp. 1-6.

[6] N. Shafiei, M. Pahlevaninezhad, and H. Farzanehfard, A. Bakhshai, P. Jain, "Analysis of a Fifth-Order Resonant Converter for High-Voltage DC Power Supplies", *IEEE Transactions on Power Electronics*, Vol. 28, no. 1, pp. 85 – 100, 2013.

[7] H. B. Kotte and R. Ambatipudi, K. Bertilsson, "High-Speed (MHz) Series Resonant Converter (SRC) Using Multilayered Coreless Printed Circuit Board (PCB) Step-Down Power Transformer", *IEEE Transactions on Power Electronics*, vol. 28, no. 3, pp. 1253 – 1264, 2013.

[8] D.C. Hamill and K.N. Bateson, "Design oriented analysis of a resonant ZVS/ZCS DC-DC converter", in Proc. of 5th European Conference on Power Electronics and Applications (EPE), 1993, pp. 23-29.

[9] H. Pollock and J.O. Flower, "New Method of Power Control for Series-Parallel Load-Resonant Converters Maintaining Zero-Current", *IEEE Transactions on Power Electronics*, vol. 12, no 1, pp. 103-115, 1997.